Tearing mode stabilization by electron cyclotron resonant heating in EAST tokamak experiments

Y. Zhang[1], X. J. Wang[*1], X. D. Zhang[*1], H. D. Xu[1], S. Gu[1], T. F. Zhou[1], T. H. Shi[1], H. Q. Liu[1], X.J. Wang[1], H. H. Wang[1], Q. Zang[1], Z. P. Luo[1], L. Q. Xu[1], R. J. Zhou[1], M. Xu[1], L. Q. Hu[1], Y. W. Sun[1], J. P. Qian[1], X. Z. Gong[1], Q. Yu[2] and EAST team

[1]*Institute of Plasma Physics, Hefei Institute of Physical Science, Chinese Academy of Sciences, Hefei 230031, China*
[2]*Max-Planck-Institut für Plasmaphysik, D-85748 Garching, Germany*

Email: xiaojing.wang@ipp.ac.cn; xdzhang@ipp.ac.cn

Abstract

The tearing mode stabilization by electron cyclotron wave (ECW) has been carried out in EAST tokamak experiments. The effects of the amount of ECW power and the radial wave deposition location on stabilizing the m/n=2/1 magnetic island are investigated, where m/n is the poloidal/toroidal mode number. The local heating is found to dominate the mode stabilization in these experiments. The stabilization is more effective when the wave is deposited closer to the radial island location, as expected. With increasing the ECW power, however, the tearing modes are not stabilized completely, and the island width saturates at a finite width. Moreover, the island rotation frequency is found to be decreased when the ECW deposition is close to the island such that the island width is reduced significantly. Using externally applied rotating resonant magnetic perturbations to generate slowly rotating magnetic islands, the locked island stabilization by ECRH has also been studied, and the island width reduction and nonuniform island rotation are observed when the island's center passes through the ECW deposition region.

1. Introduction

It is well known that the low m/n tearing modes, especially the m/n= 2/1 mode, can grow to large amplitude and possibly cause mode locking and major disruption in tokamak discharges, where m/n is the poloidal/toroidal mode number. The tearing mode can become unstable for unfavorable plasma current density profiles, which is usually the case for the plasma operating near the density limit [1-3] with relatively low electron temperature near the plasma edge [4, 5]. Even if the tearing mode was originally stable in a discharge, it can be destabilized by the error field and becomes a locked mode [6, 7], especially in discharges with low plasma rotation velocity [8]. For high beta plasmas, the perturbed bootstrap current can drive the mode growth, leading to the neoclassical tearing modes [9], which degrade the plasma confinement in both standard ELMy H–mode and advanced tokamak scenarios. Therefore, tearing modes and/or neoclassical tearing modes should be stabilized in a fusion reactor. The electron cyclotron wave (ECW) is an effective approach to the tearing mode stabilization due to its localized power deposition, as shown in the electron cyclotron resonant heating (ECRH) and/or the electron cyclotron current drive (ECCD) experiments on ASDEX Upgrade [10, 11], DIII-D [12, 13], JT-60U [14], TEXTOR [15, 16], TCV[17].

It is well known that localized current drive to increase the plasma current density at the magnetic island's O-point is stabilizing for the tearing mode. When the local electron temperature inside an island is increased by ECRH, it results in a smaller local plasma resistivity and a corresponding larger plasma current density in tokamak experiments with a toroidal inductive electric field, which is equivalent to a local current drive in the plasma current direction. The heating effect is governed by the local power deposition profiles and the heat transport across an island. Numerical simulations [18] indicate that ECRH is more efficient for suppressing a larger island in a lower electron temperature plasma, as observed in TEXTOR experiments [15, 16], while the ECCD dominates the mode stabilization in the opposite case. The ECRH contribution to mode stabilization is found to be not negligible even when extrapolating to ITER, accounting for part of the stabilizing effect for a large island [19]. ECRH has also been used to avoid major disruptions near the density limit by stabilizing large islands [20, 21]. Therefore, a better understanding of the stabilization of magnetic island by ECRH in different experimental conditions is necessary.

EAST (Experimental Advanced Superconducting Tokamak) usually operates in the regime with dominant RF heating, with a major/minor radius R = 1.85 / a = 0.45m. The m/n=2/1 tearing modes are often observed in experiments with low hybrid wave (LHW) heating, sometimes triggered by other instabilities [22]. For stabilizing magnetic islands on EAST tokamak, an ECW system (140 GHz) has been built up. In this paper, the major experimental results of the 2/1 magnetic island stabilization by ECW on EAST are reported for the first time. Two types of experiments, to stabilize the tearing modes in LHW heated discharges, driven to grow by unstable plasma current density profiles, and the slowly rotating magnetic islands generated by externally applied resonant magnetic perturbation (RMP) in Ohmic discharges, have been carried out. The results reveal that the local heating effect plays a dominant role on the mode stabilization in our experiments with a relatively low electron temperature. The stabilization is more effective when the wave is deposited near the island, as expected, but the stabilizing effect saturates with increasing ECW power. The island rotation frequency is found to be changed by ECW in the first type experiments. In the stabilization of rotating islands locked to the RMP, the decrease of the island width as well as nonuniform island rotation are observed when the island's center passes through the ECW deposition region.

In the next section our experimental setup is introduced. The stabilization of the spontaneously growing tearing modes in LHW heated discharges by ECRH/ECCD is described in Sections 3, followed by the results on the stabilization of rotating islands locked to the RMP in Section 4. A final summary is given in Section 5.

2. Experimental setup

The ECW system of EAST operates at the second harmonic of the extraordinary mode (X2-mode) [23]. It has 4 steerable mirrors installed at the major radius R = 3.0 m and the vertical position Z = +/- 0.3 m at the M-port of the machine. The steerable mirror can be adjusted from 205° to 155° in the toroidal direction and from 95° to 65° in the poloidal direction, allowing the ECW power to be deposited in the plasma region from 0.1 - 0.8 a. The first gyrotron was successfully commissioned in 2015, from which the maximum power of 500 kW can be output and modulated at a frequency of 100 Hz. This gyrotron is used to stabilize the m/n=2/1 island in our experiments. The RMP system on EAST tokamak is composed of eight upper and lower coils to generate flexible

spectrum from n = 1 to n = 4 [24]. In the second type of our experiments, RMPs with a dominant n = 1 component are used to generate a slowly rotating m/n = 2/1 island at a frequency of 10 Hz in Ohmic plasmas being originally stable to the 2/1 mode.

In addition to a poloidal array of magnetic pick-up coils (MCs), a toroidal array of 16 MCs, installed at the midplane and separated by 22.5°, is also used to measure the poloidal magnetic field perturbations. The electron cryotron emission (ECE) diagnostic has 48 channels with a time resolution of 10 μs and a radial resolution about 1 - 2 cm [25], which is used to identify the island and ECW deposition position in the experiments without LHW heating. The radial location of the q = 2 surface is obtained from the reconstruction of q-profile in the experiments with LHW, in which the ECE data are not reliable. For measuring the q-profile, a multi-channel far-infrared laser-based POlarimeter - INTerferometer (POINT) system [26] has been installed. It has 11 horizontal chords across the plasma to measure Faraday rotation angle with a phase resolution < 0.1°. The safety factor (q) profile is reconstructed using EFIT code constrained by the POINT measurement [27].

The toroidal arrangement of control tools and diagnostics is shown in figure 1, including 16 magnetic coils and 8 RMP coils. The ECE and POINT diagnostics (green star and blue diamond) locate at ϕ = -11.25° and -33.75°. The ECW launcher is installed at ϕ = -78.75° (gray square), and its power deposition location on the high field side (HFS) is mapped into the midplane of the low field side (LFS), marked by a red square. We define the middle between P and A port as the zero toroidal angle (ϕ = 0°) and the midplane on the LFS as the zero poloidal angle (θ = 0°).

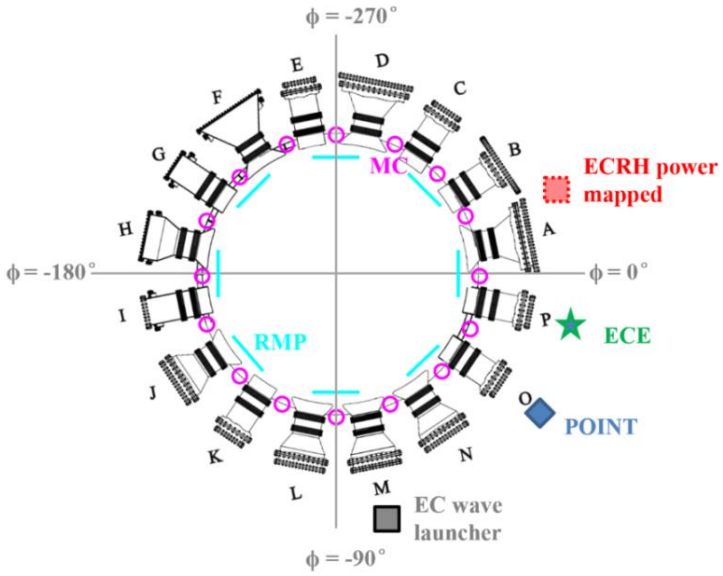

Figure 1. Top view of the toroidal location of the ECE diagnostic (green star), POINT (blue diamond), MCs (magenta circles), ECRH launcher (gray square), the mapped wave deposition location on LFS (red dotted square), and RMP coils (cyan sticks).

3. Stabilization of m/n=2/1 tearing mode in LHW discharges

LHW provides the major additional heating and current drive in EAST experiments. The m/n =2/1 tearing modes often grow spontaneously in discharges with the application of LHW of 2.45 GHz. This is consistent with the calculation result of TM1 code [46] using the experimental q-profile as input, which shows that the m/n=2/1 mode grows even without including the bootstrap current perturbation, as shown in figure 2. Our target plasmas are L-mode discharges with 1 MW LHW

heating. The plasma parameters are I_p ~ 400 kA, n_{e0} ~ 2.0×10^{19} m^{-3}, T_{e0} ~ 1.5 keV, B_{t0} ~ 2.2 T, and q_{95} ~ 5. The q = 2 surface is located at the normalized minor radius ρ_s ~ 0.6 from the q-profile reconstruction. The local poloidal plasma beta is low, β_p ~ 0.09, corresponding to a bootstrap current density fraction ~ 4%.

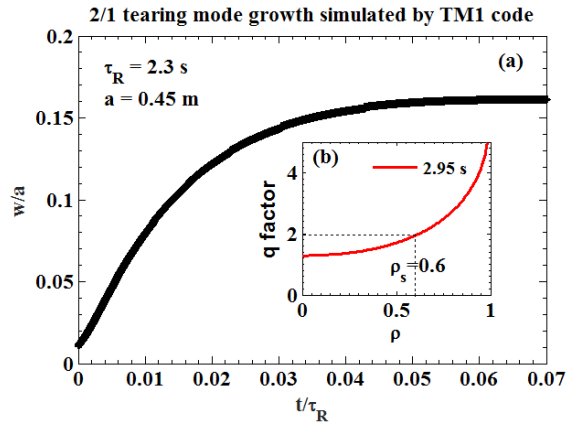

Figure 2. (a) Nonlinear time evolution of the normalized 2/1 island width simulated by TM1 code using (b) the reconstructed experimental q-profile.

An example of the mode stabilization by continuous ECW is shown in figure 3. The 2/1 tearing mode grows in the flat-top of plasma current, as shown by the MC signal in figure 3(a). The toroidal and poloidal mode numbers have been identified by MCs signals. Figure 3(b) shows the ECW waveform injected with toroidal angle of 180° and poloidal angle of 90°, hereinafter referred to as (180°, 90°), to deposit the wave near q = 2 surface. During the mode suppression, the β_N value recovers by 25% as shown in figure 3(c). The magnetic island width, calculated from $w = a_m\sqrt{\tilde{B}_{\theta m}(r_c)}$ [22], is shown in figure 3(*d*), where $\tilde{B}_{\theta m}(r_c)$ is the poloidal magnetic perturbation amplitude of the m=2 mode measured by MCs at r_c, $a_m = 4\sqrt{\frac{Rq_s r_s}{mB_{\varphi 0}s_s}\left(\frac{r_c}{r_s}\right)^{m+1}\frac{1-(r_c/r_w)^{2m}}{1+(r_c/r_w)^{2m}}} \approx 6$ cm/$\sqrt{\text{G}}$, r_s= 0.27 m (i.e. $r_s = a\rho_s$), and r_c= 0.785 m and r_w = 0.835 m are the radial location of the MCs and the vacuum vessel, derived from q profile and other experimental parameters. After the ECW is turned on, the island width first decreases from 6 to 4.5 cm in about 20 ms, followed by a slow decrease to around 3.5 cm in about 100 ms. The fast decay of the island width could be due to a more effective wave heating and electron temperature increase inside a relatively large magnetic island, while the slow decrease in about 100 ms involves in several mechanisms, to be discussed in section 3.3. The local resistive time is about 0.83 s calculated from $\tau_s = \frac{\mu_0 r_s^2}{\eta_s}$ for the local temperature T_e ~ 0.4 keV. The power spectrogram of the MC signal is shown in figure 3(e). The mode frequency does not change right after the ECW is turned on, but it has a drop from 1.6 to 1 kHz in about 20 ms when the island width is reduced to about 4.5 cm. The frequency then slowly changes even after the ECW is turned off, and it recovers only when the mode amplitude grows to a certain level (w ~ 4.5cm).

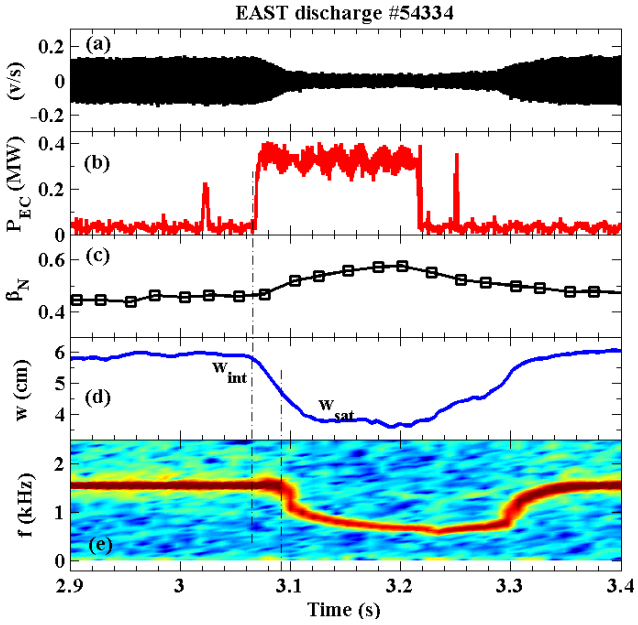

Figure 3. Stabilization of the m/n=2/1 tearing mode by continuous ECW: (a) MC signal, (b) ECW power waveform, (c) normalized β value, (d) magnetic island width, (e) power spectrogram of MC signal. The ECW is injected at the angle of (180°, 90°) to deposit wave near q = 2 surface ($\rho_s \sim 0.6$).

3.1 Effect of radial misalignment on mode stabilization

In our experiments the ECW deposition location has been changed along the minor radius by adjusting the poloidal injection angle shot by shot. The toroidal injection angles are 180°, 200° and 160°, respectively, in order to compare the resonant heating (ECRH), co-current drive (co-ECCD) and counter-current drive (counter-ECCD) effect on mode stabilization. The GA-TORAY code is used to calculate the ECW power deposition and driven current profile, as shown in figure 4 (a) and (b). For the co- and counter-ECCD case with the injection angle of (200°, 90°) and (160°, 90°), the driven current density profile has an inward Doppler shift about 0.05a compared to the power deposition profile. For the case of ECRH (180°, 90°), the wave power is deposited at $\rho_{ECH} \sim 0.56$, and the wave deposition width is about $w_{ECH} \sim 0.1a$, defined by the full width of the half maximum of power density profile. In this case the wave injection at Z = -0.3 m is not exactly perpendicularly to the magnetic field, resulting in a negligible driven current.

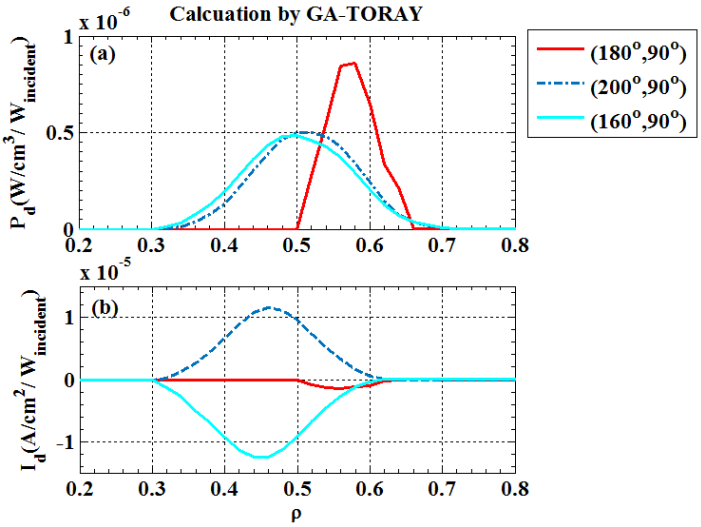

Figure 4. GA-TORAY simulation results of the radial profiles of (a) ECW power deposition density and (b) driven current density for the wave injection angle (180°, 90°), (200°, 90°) and (160°, 90°). For the case of (180°, 90°), the wave power is deposited at ρ_{ECH} ~ 0.56, with a full width of the half maximum (FWHM) of the power density profile w_{ECH} ~ 0.1 a. For the co-/counter- ECCD with (200°, 90°) / (160°, 90°), the wave power is deposited at ρ~ 0.51 / 0.50 with w_{ECH} ~ 0.18a, and the driven current position has an inward Doppler shift about 0.05a from the power deposition with the current density profile width w_{ECCD} ~ 0.15 a.

With fixed injection power of 320 kW, the mode suppression ratio, defined as the saturated island width w_{sat} after applying ECW normalized to the initial width w_{int} before applying ECW, is shown as a function of the normalized radial misalignment, $\chi_{norm,H} = \frac{(\rho_{ECH} - \rho_s)a}{\max(w_{int}, w_{ECH})}$, in figure 5(a). The discharges with ECRH are marked with red squares. It is seen that the mode suppression is most effective for the case with the smallest radial misalignment of $\chi_{norm,H}$ ~ -0.2 (#54334). The stabilization effect exists in a wide region of -1 <$\chi_{norm,H}$ <0.6, which is likely due to the large wave deposition width such that part of the wave power is still deposited inside the island, which could lead to a small increase of the local electron temperature, considering that the local temperature gradient and the perpendicular heat conduction inside the island could be small [28]. As a comparison, the co-ECCD and counter-ECCD cases are shown by the blue and cyan triangles in figure 5(a), which are close to that of ECRH cases. For $\chi_{norm,H}$ ~ -1, the mode amplitude is slightly increased in discharge #54340 by co-ECCD, possibly due to the driven current around the island's separatrix. In contrast, partial stabilization is observed for the counter-ECCD case with $\chi_{norm,H}$ ~ -1 in discharge #54341, since the counter-ECCD around the island's separatrix is stabilizing. For $\chi_{norm,H}$ <-1, the mode amplitude is increased by the heating effect. This might be caused by the increase of the electron temperature and the plasma current density gradient outside the inner edge of the island and the corresponding increase of the stability index of the tearing mode. These results are as expected from the theoretical results about the ECRH effect on the island width shown in Ref. [19].

In figure 5(b), the value of $w^* = w_{int}/w_{ECH}$ is shown as the function of $\chi_{norm,H}$. The value of w_{ECH} decreases when the ECW power deposition moves toward plasma center. It is seen that w^* >1 for all ECRH cases (squares), but w^* < 1 for co-ECCD and counter-ECCD cases.

One can conclude that the ECRH rather than the ECCD plays the major role in the mode stabilization in our experiments with relatively lower plasma temperature. In the following, we will only focus on the mode stabilization by ECRH.

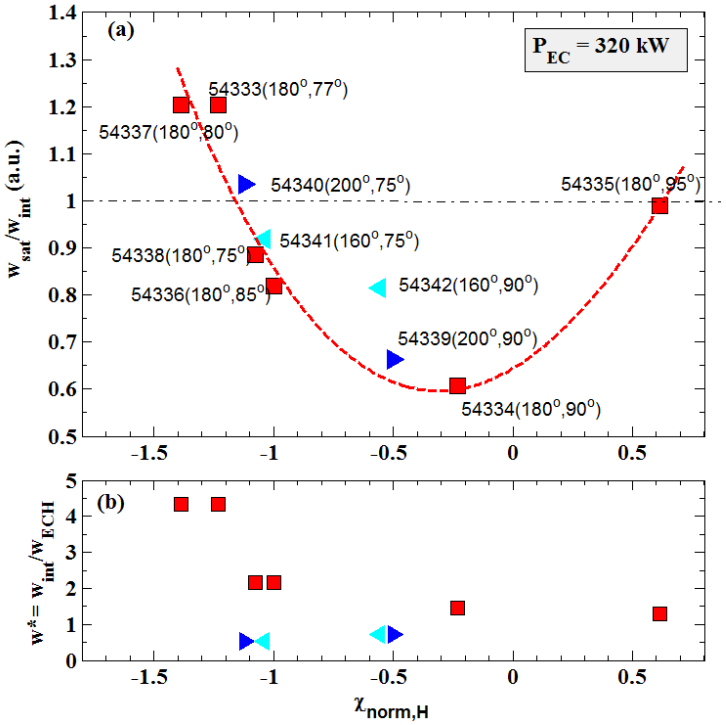

Figure 5. (a) The 2/1 mode suppression ratio as a function of the normalized radial misalignment $\chi_{norm,H}$. The ratio is defined as the saturated island width w_{sat} after applying ECW normalized to the initial width w_{int} before applying ECW. The ECRH cases are shown by red squares, and the co-ECCD and counter-ECCD cases are marked by blue and cyan triangles. The suppression is most effective for $\rho_{ECH} \sim 0.56$ being close to the $q = 2$ surface. (b) The dependence of $w^* = w_{int}/w_{ECH}$ on $\chi_{norm,H}$, indicating a smaller w_{ECH} for the ECW power deposition towards plasma center.

3.2 Effect of ECW on mode rotation

The change of mode frequency by ECW, as shown in the figure 3(e), is found to be significant only when the wave deposition is close to the island.

Figure 6 (a) - (d) show the time traces of island width and mode frequency for four discharges, with $\chi_{norm,H}$ = -1, -1.08, -1.38 and 0.61, respectively. The time period with ECRH is marked by two vertical dotted lines. For the case with $\chi_{norm,H}$ = -1 shown in figure 6(a), the mode frequency is reduced when the island width is reduced to below 4.5 cm, similar to that shown in figure 3(e). For $\chi_{norm,H}$ = -1.08 and 0.61 shown in figure 6(b) and (d), no significant reduction in mode amplitude or frequency occurs. For $\chi_{norm,H}$ = -1.38 shown in figure 6(c), the island width is increased by ECRH, but the mode frequency only slightly changes. These results indicate a correlation between the frequency change and the ECW deposition location. The island is found to rotate in the counter-I_p direction before applying ECRH from the MCs signals. The decrease of the mode frequency corresponds to a change of the island rotation towards the co-I_p direction. Such a change cannot be explained by the contribution of the electron diamagnetic drift to the mode frequency for a sufficiently small island, since this would lead to an increase rather than a decrease of the mode frequency. The mode frequency decrease observed in our experiments is opposite to

what was typically observed in NTM stabilization experiments with EC beams in DIII-D [12], JT-60U [14] and TCV [33], where the mode frequency tends to increase with decreasing island width for the plasma rotation in both the co-I_p [12] and the counter-I_p [14] directions.

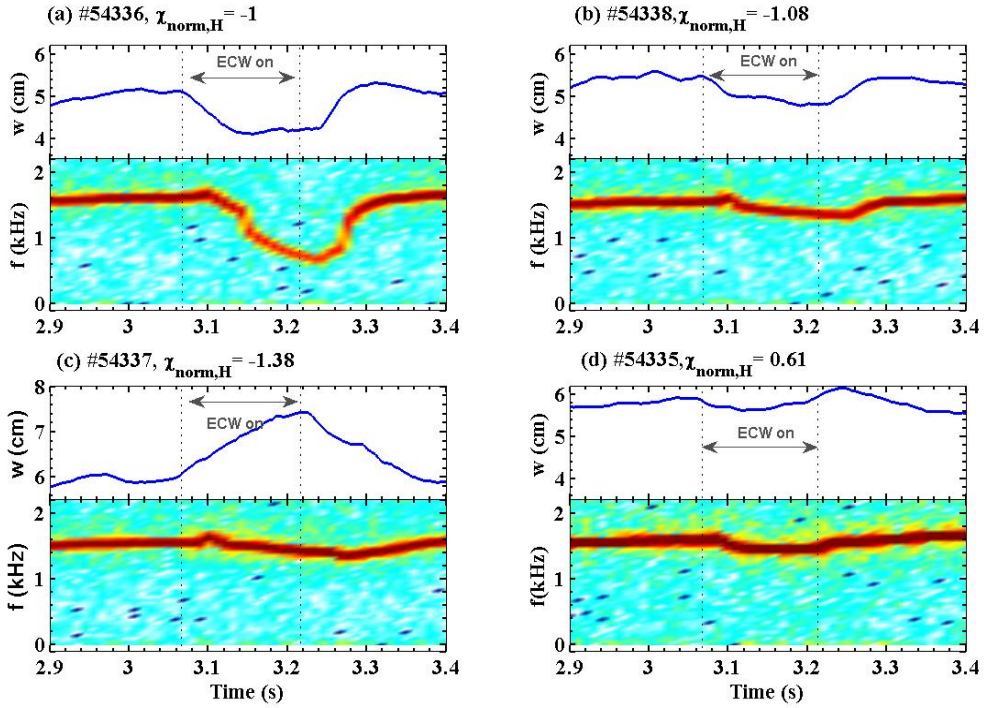

Figure 6. Time traces of mode amplitude and frequency for four discharges, with $x_{norm,H}$ = -1, -1.08, -1.38, 0.61, respectively. The time period with ECRH is marked by two vertical dotted lines.

It is well known that RF heating can change the plasma rotation velocity [29-31], i.e., the so-called intrinsic torque [32]. Our results reveal that, however, the change of the island rotation velocity by ECW depends on the island width reduction. The electromagnetic torque due to the eddy currents in the wall had been utilized for explaining the change of the mode frequency in ECRH/ECCD experiments [35]. This mechanism qualitatively agrees the increase of mode frequency with decreasing island width observed in other tokamak experiments [12, 14, 33], but it cannot explain the frequency decrease with decreasing island width in our experiment, since the electromagnetic torque to slowdown the mode rotation is proportional to the 4th power of the island width.

The plasma rotation had also been considered to be affected by the mode itself via NTV torque [34]. The NTV torque has been calculated using our experimental data and the NTVTOK code [36], showing that the torque is in the counter-I_p direction and decreases with decreasing island width. This is in line with the results shown in figures 3(e) and 6(a), since the plasma rotation is in the counter-I_p direction. However, the result shown in figure 6(c) contradicts this explanation, because no mode frequency increases is observed with increasing island width. The mechanism for the correlation between the frequency change and the island width, as well as the observed threshold in the island width, remains not clear yet.

3.3 Effect of ECW power on mode stabilization

The effect of the amount of the ECRH power on mode stabilization has been investigated by

fixing the injection angle of (180°, 90°) to deposit the wave around $\rho_{ECH} \sim 0.56$. Figure 7 presents the ratio of w_{sat}/w_{int} as a function of the input ECRH power (red squares). The m/n = 2/1 tearing mode is partly stabilized with only 100 kW wave power, being about 0.066 of the total heating power. The island width decreases with increasing ECRH power but almost saturates when the power is increased to about 320 kW. The tearing mode has not been suppressed completely by ECRH. The ECW power deposition width is about 4.5 cm, being larger than the minimum saturated island width 3.5 cm in discharge #54334. The poloidal β is increased by about 25% with the highest ECW power, and the local bootstrap current density fraction is about 5% in this case.

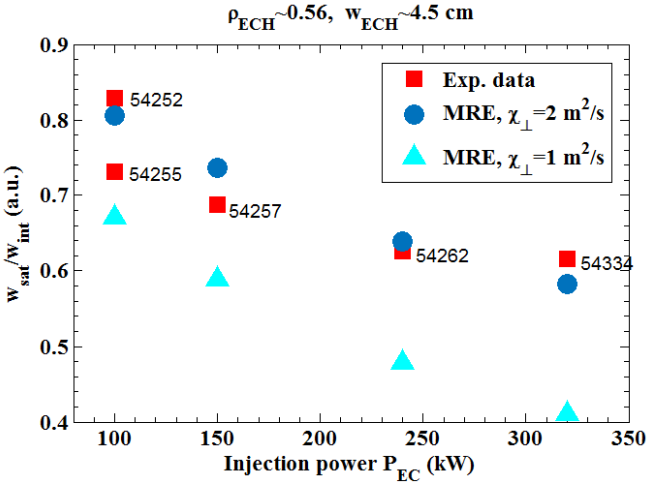

Figure 7. The 2/1 mode suppression ratio w_{sat}/w_{int} as a function of the ECRH power. The red squares are experiment results, and the circles and triangles are obtained from the MRE with $\chi_\perp = 2\ m^2/\text{s}$ and $1\ m^2/\text{s}$, respectively.

To compare with experimental results, the modified Rutherford equation (MRE) [41]

$$0.82\frac{\tau_s}{r_s}\frac{dw}{dt} = \Delta_0' r_s + \Delta_{bs}' r_s - \Delta_H' r_s$$

is utilized. The first term on the right hand side of the equation, $\Delta_0' r_s$, is the tearing mode stability index obtained from the reconstructed experimental q-profile, and its dependence on the island width is calculated during the nonlinear mode growth from TM1 code simulation, as shown in figure 2. The 2nd term, $\Delta_{bs}' r_s \approx -\beta_p a_{bs}\frac{r_s}{w}\frac{w^2}{w^2+w_d^2}$ [39], is due to the bootstrap current perturbation, where $a_{bs} \sim 3.0$ and $w_d = 1.8 w_c$ [37], $w_c = \sqrt{8} r_s (1/\varepsilon_s s_s n)^{1/2} (\chi_\perp/\chi_{//})^{1/4} \sim 2$ cm is the marginal island width for the perpendicular heat transport across an island, calculated from the experimental data: $r_s \sim 0.27$ m, the local magnetic shear $s_s \sim 1.07$, and the local inverse aspect ratio $\varepsilon_s \sim 0.14$. The value of the saturated island width is larger than w_c. The parallel thermal conductivity is $\chi_{//} = v_{Te}/k_b \sim 1.13\times10^8$ m/s [38] for the local temperature $T_e \sim 0.4$ keV and the island width $w \sim 3.5$ cm, where v_{Te} is the electron thermal speed, $k_b \sim nw/RL_{qs}$ the parallel wave vector and $L_{qs} \sim r_s/s_s$ the shear length. The perpendicularly thermal conductivity is assumed to be $\chi_\perp = 2\ m^2/\text{s}$. The 3rd term on the right hand side of MRE, $\Delta_H' r_s \approx \frac{16\mu_0 L_q}{B_p \pi}\frac{\eta_H P_{tot}}{w_{ECH}^2} F_H(w^*, x_{ECH})$ [19, 40],

is due to ECRH effect, where $F_H(w^*, x_{ECH})$ is a function of $w^*=w/w_{ECH}$ and $x_{ECH} = r_s - r_{ECH}$, $\eta_H = \frac{3w_{ECH}^2}{8\pi R n_{e,s}\chi_\perp K_B}\frac{j_{sep}}{T_{sep}}$, $n_{e,s}$ is the local electron density, j_{sep} the current density at the island separatrix, and T_{sep} the electron temperature.

In the Figure 8(a), the values of these three terms in the MRE are shown as function of island width. The values of $\Delta_H' r_s$ and $\Delta_{bs}' r_s$ are plotted for different injection power. One can see that as the island width decreases, the ECRH effect decreases, while the value of $\Delta_0' r_s$ increases. Due to the low bootstrap current fraction, the bootstrap current perturbation is not important for a sufficiently small island, and it is smaller than the heating effect for a sufficiently large island. Nevertheless, it can still contribute to the saturated island width when the island width is reduced by ECRH to approach $w \sim w_d$. The normalized saturated island widths obtained from the MRE with $\chi_\perp = 2\, m^2/\mathrm{s}$ are also shown in figure 7 by circles, which approximately agrees with the experimental ones. It should be mentioned that, however, the values of $\Delta_H' r_s$ depend on the local value of $\chi_\perp$ in the island region, which is subjected to certain level of uncertainty and could be affected by the ECRH. As a comparison, the results obtained from the MRE for $\chi_\perp = 1\, m^2/\mathrm{s}$ is also shown in figure 7.

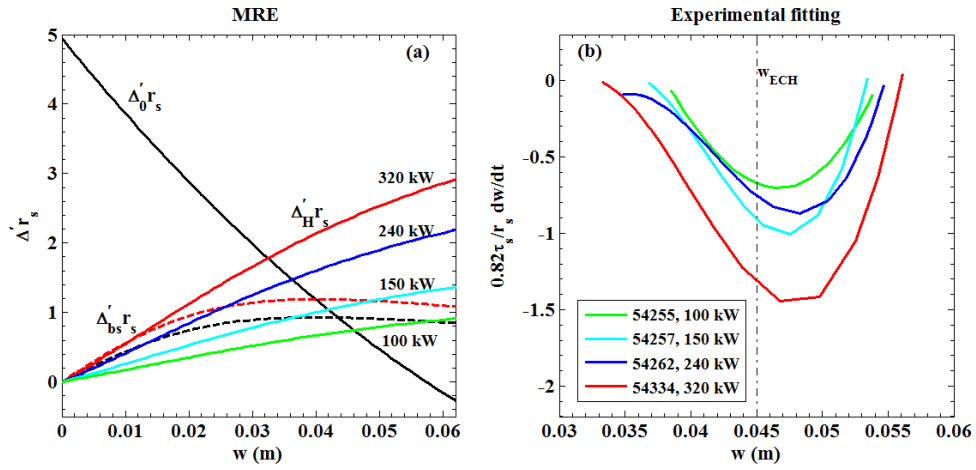

Figure 8. (a) The values of $\Delta_0' r_s$, the heating term $\Delta_H' r_s$ and bootstrap current term $\Delta_{bs}' r_s$ in the MRE calculated using experimental data with $\chi_\perp = 2\, m^2/\mathrm{s}$. The values of $\Delta_H' r_s$ are plotted by solid lines for different injection power. The values of $\Delta_{bs}' r_s$ without ECRH and with 320 kW ECRH power are shown by black and red dashed curves. (b) The value of $(0.82\tau_s / r_s)\, dw/dt$, derived from the experimental data, is shown as function of island width for different ECW power.

The time traces of $(0.82\tau_s / r_s) dw/dt$, derived from the experimental data, are shown as function of island width in Figure 8(b), where τ_s = 0.83 s. It is seen that the minimum value of dw/dt is around $w \sim 4.7$ cm, being slightly larger than $w_{ECH} \sim 4.5$ cm for the ECRH cases, implying a more effective heating and stabilizing effect on the mode for $w > w_{ECH}$. When the island width further decreases, the increase in the value of dw/dt can be explained by the following reasons: (1) The fraction of the wave power deposited inside the island decreases as $w < w_{ECH}$; (2) The difference between the electron temperature at the center and the X-point of an island is smaller for a smaller island even for the same amount of the ECRH power deposited inside an

island [42]; (3) The tearing mode stability index, Δ_0', increases with decreasing island width, as seen from figure 8 (a); (4) The bootstrap current effect increases when the island width is reduced by ECRH to approach $w \sim w_d$.

It is seen that the ECRH is effective for reducing the width of a large island, but the stabilizing effect decreases for a small island.

4. Stabilization of n = 1 island locked to rotating RMP

It is well known that sufficiently large applied RMPs can generate magnetic islands inside the plasmas for which the tearing mode was originally stable. The generated island will be approximately in phase with the RMP due to the applied electromagnetic torque, being proportional to the RMP amplitude and the square of the island width [44], despite that the surrounding plasma outside the island might still rotate. When the applied RMP and the generated island slowly rotates, it allows to study the island stabilization by ECRH in more detail, in particular about the effect of the ECW deposition along the helical angle.

For this purpose, a reference discharge with RMP but without ECRH has firstly been carried out in Ohmic discharge with the following plasma parameters: $I_p \sim 500$ kA, $n_{e0} \sim 1.5\times10^{19}$ m^{-3}, $T_{e0} \sim 1.0$ keV, $B_{t0} \sim -2.4$ T, and $q_{95} \sim 5.6$. There is no tearing mode in this discharge without applying RMPs. Figure 9(a) shows the waveform of applied RMP coil current I_{RMP} in this experiment. Even connection with zero phase difference between the upper and lower RMP coils is adopted to generate a RMP spectrum dominated by the n = 1 component. A static RMP is first applied, and then it rotates in the counter-I_p direction at a frequency of 10 Hz. The generated m/n = 2/1 island rotates following the RMP rotation. Due to the low rotation frequency of the island, the magnetic perturbation is evident in the MC signal only after RMP coil current is switched off at t = 4.0 s, as shown the figure 9(b), when the island unlocks from RMPs and begins to rotate. Afterwards the perturbation decays in about 30 ms, since the plasma was originally stable to the 2/1 mode. The local resistive time is about 0.36 s, calculated from $\tau_s = \frac{\mu_0 r_s^2}{\eta_s}$. The poloidal magnetic perturbation of the n = 1 component, $B_{p,n=1}$, is measured by MCs and calculated from Fourier decomposition. Figure 9(c) shows the time evolution of $B_{p,n=1}$ along the toroidal angle, from which the RMP vacuum field and eddy current contributions have been excluded. The red and blue colors correspond to the island's X- and O-points. Figure 9(d) presents the electron temperature measured by five ECE channels viewing near the magnetic island, from which the component with a frequency higher than 10 Hz has been excluded. The 2/1 magnetic island locates at about R = 2.149 m, identified by the distorted sinusoidal temperature perturbation and the π phase reverse of signals on its opposite sides. The ECE channel at R = 2.128 m passes through the island separatrix from the inner side of the q = 2 surface, so that the measured temperature has the maximum at the phase of the X-point, and it increases towards the center of the magnetic island, resulting in an additional small peak [43]. The phases of the island's X and O points are marked with 'x' and 'o' symbols in this signal, which agree with the maximum and minimum amplitude of $B_{p,n=1}$ viewed at the ECE location (ϕ_{ECE} = -11.25°), as marked in figure 9(c).

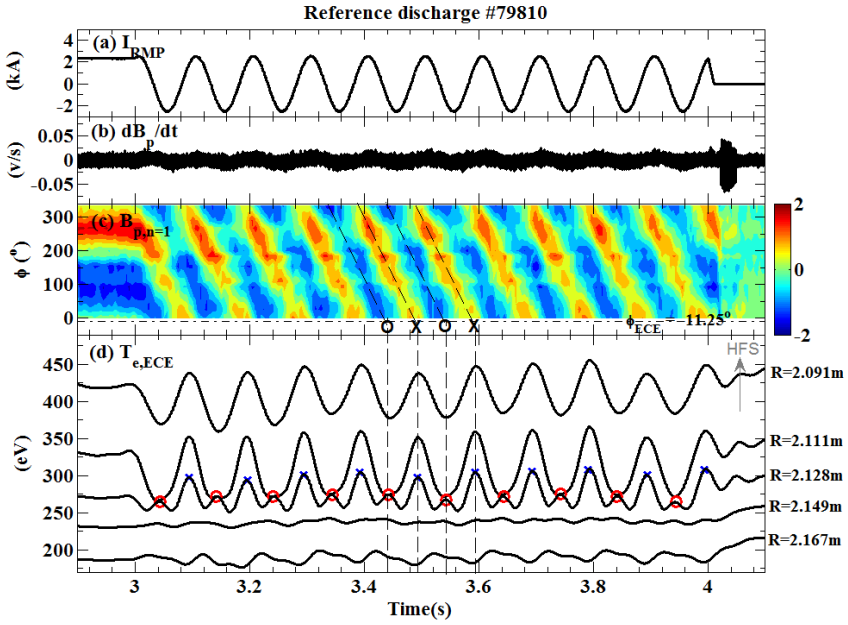

Figure 9. For the reference discharge (#79810) without ECRH: (a) RMP coil current waveform; (b) MC signal; (c) contour of the poloidal magnetic perturbation of n = 1 component, measured by MCs on the mid-plane, excluding the RMP vacuum field and eddy current contributions; (d) electron temperature measured by five ECE channels near the island, excluding the component with a frequency higher than 10 Hz. The phases of the island's X- and O- points viewed by the ECE channel at R = 2.128 m, passing through the island on the inner side of q = 2 surface, are marked with 'x' and 'o' symbols. They agree with the X- and O-points identified by the magnetic perturbation shown in (c) at ECE viewing location ϕ_{ECE} = -11.25° (marked by dot-dashed line).

For the fourth period of island rotation, the electron temperature profiles measured at the phases of island's O- and X-points are shown in figure 10(a). A local flattening of the temperature profile is observed at the phase of the O-point, which locates on the inner side of R = 2.149 m. The possible causes of the flattening shifts with respect to the 2/1 surface are: (1) the O-point of the magnetic island usually shifts inward with respect to the resonant surface [46]; (2) the spatial resolution of ECE channels viewing around the q = 2 surface is limited to about 2 cm, as shown in figure 9(d), which could be larger than the half width of the magnetic island. The temperature at the O-point phase is lower than that at the X-point phase by 10%. It is found from the figure 10(a) and 9(d) that the island width is about 3.8 cm (+/- 0.5 cm) for $|B_{n=1}|$ ~ 1 G, leading to a factor of $c_0 = 3.8\text{cm}/\sqrt{\text{G}}$ for calculating the island width from $|B_{p,n=1}|$ in the following. The island width calculated from magnetic measurement using the formula in Section 3 is about w ~ 4.3 cm, being comparable to that seen from ECE. Figure 10(b) shows the q-profiles at two different times with and without ECRH, obtained from equilibrium reconstruction with EFIT code constrained by POINT measurement. They have been transferred from flux to geometry coordinate (i.e. $\rho \rightarrow R$) for comparison to ECE measurement. The locations of the q = 2 surface differ by about 2 cm from the ECE data.

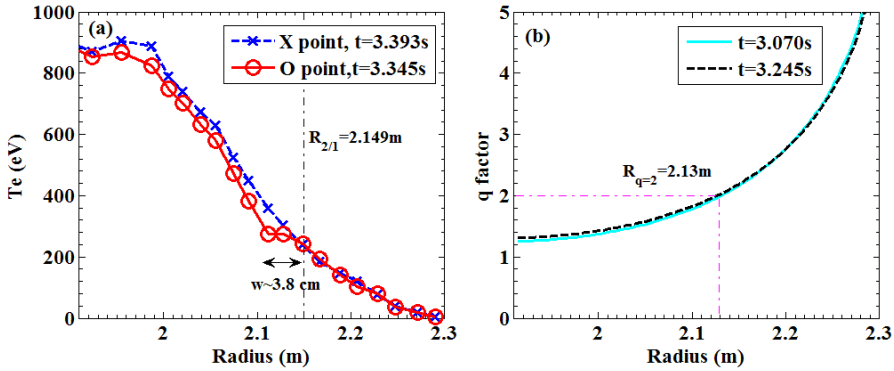

Figure 10. (a) Radial profile of electron temperature at the phase of island's X- and O-point for the fourth rotation period shown in figure 9(d); (b) The q profiles obtained from equilibrium reconstruction with EFIT code and POINT data.

In the discharges with ECRH application, same plasma parameters and the RMP coil current waveform have been utilized. The ECW power is modulated between 200 and 400 kW at a frequency of 50 Hz with 50% duty-cycle for diagnostic purpose, as shown in figure 11(a). The ECRH power deposition position R_{ECH} is measured by the maximum amplitude and phase delay of the resultant temperature perturbation [44], utilized to calculate the radial misalignment between ECW deposition and island location, $\Delta r = R_{ECH} - R_{2/1}$. The predicted wave deposition from TORAY-code agrees with that from the ECE measurement within the experimental measurement error bar. Figure 11 (b) - (d) show the island suppression by ECRH in a discharge with $\Delta r = +1.5$ cm. In figure 11 (b), the amplitude $|B_{p,n=1}|$ for reference discharge without ECRH (#79810) is shown by black curve, being about 1.5 G during static RMP phase and decreasing to about 1 G after the island begins to rotate. A small oscillation in the amplitude is caused by the plasma displacement. When the ECRH is applied, $|B_{p,n=1}|$ is reduced to about 0.5 G, as shown by red curve, and it recovers after ECRH is turned off. Figure 11 (c) shows the toroidal phase of island's X-point, $\phi_{p,n=1}$, starting from -90° and then rotating in the contour-I_p direction, following the RMP rotation. The mode rotation becomes non-uniform in the presence of ECW. Figure 11 (d) and (e) show the contour plots of $B_{p,n=1}$ without and with ECRH, excluding the RMP vacuum field and eddy current contributions. Compared to the reference discharge, the amplitude of $B_{p,n=1}$ is significantly reduced by ECRH, especially when the magnetic island's O point passes through the ECRH power deposition at $\phi_{ECH,LFS} \sim 21.6°$, which has been mapped from the ECW resonance on HFS to the mid-plane on LFS along the field line, as marked by the dashed line in figure 11(e).

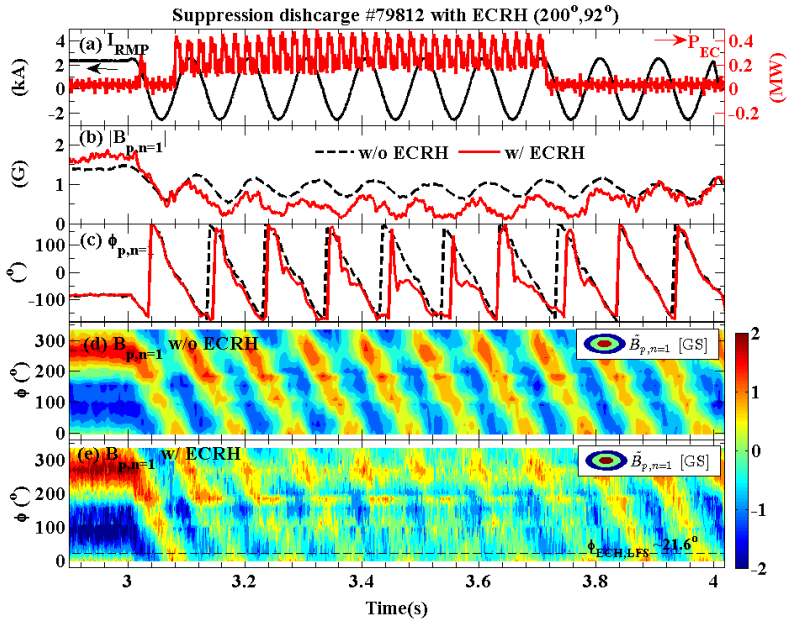

Figure 11. ECRH effect on the island locked by rotating RMP in discharge of #79812: (a) RMP coil current and applied ECW power; (b) magnitude and (c) toroidal phase of poloidal magnetic perturbation of n = 1 component (red curves), compared to those without ECRH (black dashed curves); (d) and (e) contour plot of $B_{p,n=1}$ without and with ECRH, measured by MCs on the mid-plane, excluding the RMP vacuum field and eddy current contributions. The ECRH power deposition mapped to the midplane on the low field side, $\phi_{ECH,LFS}$, is marked by the black dashed line in (e).

Figure 12 presents the island width reduction by ECRH with two different radial misaglinements, Δr = +1.5 and -6.0 cm, obtained in two discharges, where the island width is calculated from $w = c_0\sqrt{|B_{p,n=1}|}$ with $c_0 = 3.8$ mentioned before, and the island width reduction is defined as $\Delta w = w_{\rm sup} - w_{\rm ref}$, with $w_{\rm sup}$ and $w_{\rm ref}$ being the island width in the discharge with and without ECRH, respectively. Basing on the time traces shown by figure 11(b) and (c), the island width for each discharge has been shown as a function of the toroidal island phase, interpolating with the equal interval of 0.1π. The negative increase of $\phi_{p,n=1}$ indicates the island rotation in counter-I_p direction. The time period with ECRH is marked with gray box. For reader's convenience, the contour of the helical flux of Ω = 1 and -0.5 are plotted along $\phi_{p,n=1}$ to show the island's separatrix and O-point region, where $\Omega = 8(r-r_s)^2/w^2 + \cos\xi$ [37], $w = w_{ref}$ and $\xi = m\theta - n\phi_{p,n=1}$. As shown by Figure 11(c), the phase of island's X-point starts at $\phi_{p,n=1} = -0.5\pi$ before t = 3.0 s, leading to $m\theta$ = -0.5π.

It is seen from figure 12 that after the ECRH is turned on for the discharge with Δr = +1.5 cm, the island width periodically decreases, and $|\Delta w| \sim 2.0$ cm is reached in the fourth rotation period (in a time period about 300 ms), corresponding to a suppression ratio of $w_{sup}/w_{ref} \sim 47\%$. As the island rotates with respect to the wave deposition region ($\phi_{ECH,LFS}/2\pi \sim 0.06$), the island width is reduced only when the island's O point passes through the wave deposition region, while it increases when the wave deposition is around the X-point. This confirms that the local heating

inside the island is stabilizing, as expected. For the discharge with a larger radial misalignment, Δr = -6.0 cm, the island width reduction is smaller, and no obvious correlation between the minimum island width and the ECW deposition around the O-point phase is observed. After the ECRH is turned off, the stabilization effect lasts for about 1-2 rotation periods for the case Δr = +1.5 cm, implying a good energy confinement inside the island so that a higher local electron temperature is maintained for about 200 ms. However, the change of the plasma current density profile on a local resistive timescale might also play a role for the slow recovery of mode amplitude after the ECRH is turned off.

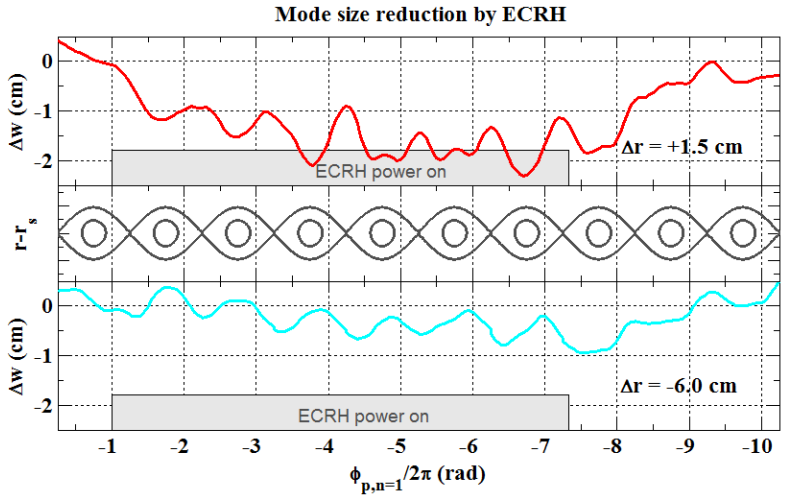

Figure 12. Reduction of island width $\Delta w = w_{sup} - w_{ref}$ as a function of $\phi_{p,n=1}$ for two discharges with the radial misalignment Δr = +1.5 and -6.0 cm, respectively. A cartoon picture of the helical flux with Ω = 1 and -0.5 are plotted along the toroidal angle to show the island's separatrix and O-point region. The time period with ECRH is marked with gray box.

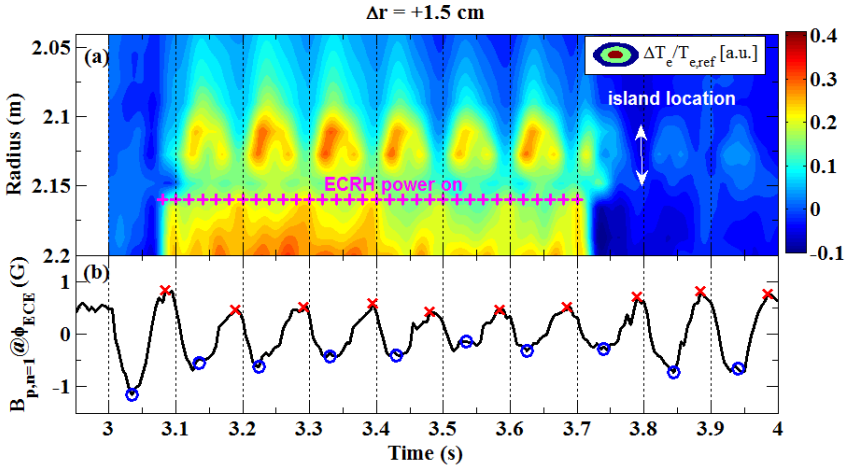

Figure 13. (a) Contour of the relative temperature difference between the discharge with Δr = + 1.5 cm and the reference discharge without ECRH, where the time period with ECRH application is marked by '+' at its power deposition R_{ECH}~2.16 m; (b) The poloidal magnetic perturbation viewed at the ECE installation of ϕ_{ECE} = -11.25°, where the phases of island's O and X points are marked with 'o' and 'x' symbols.

Figure 13 (a) shows the contour of the relative temperature difference between the discharge with ECRH at Δr = + 1.5 cm and the reference discharge without ECRH. The poloidal magnetic

perturbation, viewed at the ECE installation of ϕ_{ECE} = -11.25°, is shown in Figure 13(b), where the phase of island's O and X points are marked. One can see that a slightly higher local electron temperature in the island region between R = 2.15 m and R = 2.11 m is maintained for about two rotation periods after turning off the ECRH power.

In the reference discharge without ECRH, the island rotates with a frequency of 10 Hz in the counter-I_p direction, being the same as the RMP rotation. The island rotation is found to be modulated by ECRH only when the island width is reduced significantly by ECRH. Figure 14 (a) is the same as figure 11(c) but shows the toroidal phase of n = 1 poloidal magnetic perturbation in a shorter time window for two cases, with (red solid curves) and without ECRH (black dashed curves). The corresponding time evolution of the phase velocity (instantaneous frequency) of the island rotation, defined as $f = d\phi_{p,n=1}/dt$, is shown in Figure 14 (b). After ECRH is turned on for the discharge with Δr = + 1.5 cm, $f \sim$ -80 Hz is observed when the island's O-point passes through the ECW deposition region, corresponding to a rotation acceleration in the counter-I_p direction. The nonuniform island rotation is obvious only for a larger island width reduction with a smaller radial misalignment. For the discharge with Δr = -6.0 cm, there is no significant change in the phase velocity.

The nonuniform island rotation can be understood in the following way. After turning off RMPs at t = 4.0 s, the island is found to rotate at a frequency of 0.7 kHz in the counter-I_p direction from the MC signals, as shown in figure 9(b). This indicates that the surrounding plasma outside the island rotates in this direction. When the island width is reduced by ECRH, the electromagnetic torque applied from RMPs to lock the island decreases, similar to that by switching off RMPs. Therefore, the viscous torque from surrounding plasma will tend to drive the plasma inside the island together with the island to rotate in the counter-I_p direction. When the island's X-point passes through the ECW deposition, the island width and the electromagnetic torque increase, forcing the island to rotate together with the applied RMP again. In addition, the surrounding plasma rotation velocity might also be decreased during the ECRH phase, similar to that shown in figure 3, which will lead to a decreased viscous torque, since this torque is proportional to the plasma velocity outside the island.

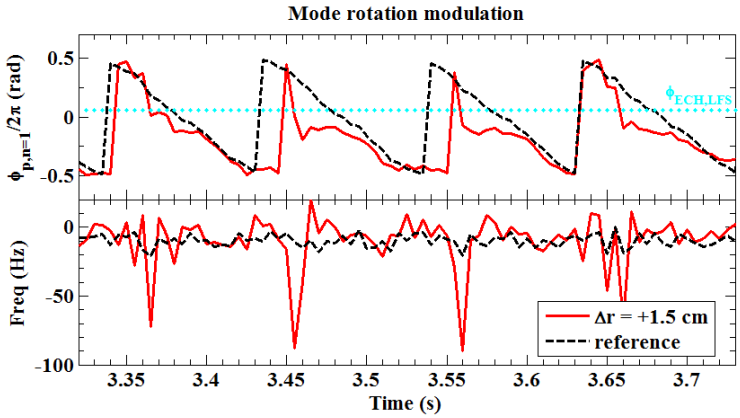

Figure 14. (a) Same as figure 11(c) but show the toroidal phase of n = 1 poloidal magnetic perturbation in a shorter time window with (red curves) and without ECRH (black dashed curves). The mapped phase of ECRH power deposition on LFS, $\phi_{ECH,LFS}$, is marked by cyan dotted line. (b) The corresponding phase velocity (or instant frequency) of the island rotation calculated from $f = d\phi_{p,n=1}/dt$.

5. Discussion and Summary

In this paper, the results of the m/n = 2/1 island stabilization by ECW in EAST experiments are reported. Two types of experiments have been carried out. In the first type, the m/n = 2/1 tearing modes, growing spontaneously in the discharges with LHW, are partly stabilized by continuous ECRH. The experimental results show that the heating effect plays a dominant role on the mode stabilization, similar to that observed in TEXTOR experiments [15]. The mode suppression is more efficient for a smaller radial misalignment, as expected. With increasing ECW power, the mode has not been completely stabilized, which is in line with the results obtained from the MRE.

Moreover, the mode frequency is found to be decreased by about twice when the island is partly suppressed by ECRH in the first type experiments. Such a phenomenon differs from the observations in other NTM stabilization experiments by ECW [12, 14, 33]. Although it is well known that the plasma rotation can be affected by ECRH or other RF wave heating [29-31], and the mode frequency can also be affected by the electromagnetic torque due to the eddy currents in the wall [35] and the NTV torque generated by the mode itself [34], the mechanism for the correlation between the frequency decrease and the island width reduction, as well as the observed threshold in the island width for the frequency decrease observed in our experiments, remains not clear yet. As the stabilizing efficiency of ECRH/ECCD depends on the island rotation frequency [45, 46], and the effect of RF wave heating on plasma rotation is also an important issue in fusion research, future study about the effect of local ECRH at the resonant surface on plasma rotation is still required to understand the underlying physics.

In the second type of our experiments, externally applied RMPs are used to generate a slowly rotating locked island in Ohmic discharges. Both the island and ECW deposition position are measured by ECE in these discharges, so that the radial misalignment of ECW power deposition is reduced to about 1.5 cm. As the locked island slowly rotates following the RMP rotation, it is found that the island width is reduced by ECRH only when the island's O-point passes through the wave deposition region for a small radial misalignment. Nonuniform island rotation is observed in these experiments when the island width is significantly reduced by ECRH, being consistent with the decreased electromagnetic torque from RMPs for a smaller island. The island has not been unlocked from RMPs. This indicates that while the local ECRH is effective in reducing the width of a large island, local ECCD or other methods might still be required for fully stabilizing the island, as shown in the locked island stabilization experiments by ECCD [47].

Acknowledgements

This work is financially supported by the National Natural Science Foundation of China (Grant No. 11875293), by the National Magnetic Confinement Fusion Science Program of China under Contracts No. 2012GB103003, and by project No. 2019HSC-UE015.

Reference

[1] M. Greenwald, *Plasma Phys. Control. Fusion* **44** (2002), R27–R80.
[2] G. K. Robert, and J. F. Drake, *Phys. Fluids* **3** (1991), 020372.
[3] D. A. Gates and L. Delgado-Aparicio, *Phy. Rev. Lett.* **108** (2012), 165004.
[4] F. C. Schüller, *Plasma Phys. Control. Fusion* **37** (1995) A135.
[5] Y. Zhang, *et al*., *Nucl. Fusion* **51** (2011) 063039.

[6] R. J. La Haye, R. Fitzpatrick, *Phys. Fluids* **4** (1992) 2098.
[7] R. J. Buttery, *et al*., *Nucl. Fusion* **40** (2000) 807.
[8] G. L. Jackson, *et al.*, *Nucl. Fusion* **55** (2015) 023004.
[9] Z. Chang, *et al.*, *Phys. Plasmas* **5** (1998), 1076.
[10] M. Maraschek, *et al.*, *Nucl. Fusion* **45** (2005) 1369.
[11] M. Maraschek, *et al*., *Phy. Rev. Lett.* **98** (2007) 025005.
[12] C. C. Pretty, *et al.*, *Nucl. Fusion* **44** (2004) 243.
[13] R.J. LaHaye, *et al.*, *Nucl. Fusion* **46** (2006) 451.
[14] A. Isayama, *et al.*, *Nucl. Fusion* **49** (2009) 055006.
[15] E. Westerhof, *et al., Nucl. Fusion* **47** (2007) 85.
[16] I. G. J. Classen, *et al.*, *Phy. Rev. Lett.* **98** (2007) 035001.
[17] F. Felici, *et al, Nucl. Fusion* **52** (2012) 074001.
[18] Q. Yu and S. Günter, *Plasma Phys. Control. Fusion* **40** (1998) 1977.
[19] D. De Lazzari and E. Westerhof, *Nucl. Fusion* **49** (2009) 075002.
[20] B. Esposito, *et al.*, *Phy. Rev .Lett.* **100** (2008) 045006.
[21] B. Esposito, *et al.*, *Plasma Phys. Control. Fusion* **53** (2011) 124035.
[22] T. H. Shi, *et al., Plasma Phys. Control. Fusion* **55** (2013) 055007.
[23] X. J. Wang, *et al., Fusion Eng. Design* **96-97** (2015), 181-186.
[24] Y. Sun, *et al., Plasma Phys. Control. Fusion* **57** (2015) 045003.
[25] Y. Liu, *et al., Plasma Sci. Technol.* **13** (2011), 352-356.
[26] H. Q. Liu, *et al., Rev. Sci. Instrum*. **87** (2016) 11D903.
[27] J. P. Qian, *et al., Nucl. Fusion* **57** (2017) 036008.
[28] S. Inagaki, *et al., Phy. Rev .Lett*. **92** (2004) 055002.
[29] J. E. Rice, *et al., Nucl. Fusion* **53** (2013) 093015.
[30] J. E. Rice, *et al., Nucl. Fusion* **56** (2016) 036015.
[31] R. M. McDermott, *et al., Plasma Phys. Control. Fusion* **53** (2011), 124013.
[32] K. Ida and J.E. Rice, *Nucl. Fusion* **54** (2014) 045001.
[33] M. kong, *et al., Nucl. Fusion* **59** (2019) 076035
[34] E. Lazzaro *et al., Nucl. Fusion* **55** (2015) 093031
[35] G. Ramponi *et al., Phys. Plasmas* **6** (1999) 3561
[36] Y. Sun *et al, Nucl. Fusion* **53** (2013) 093010
[37] R. Fitzpatrick, *Phys. Plasmas* **2** (1995) 825.
[38] Q. Yu *et al., Phys. Plasmas* **7** (2000) 312.
[39] O. Sauter *et al. Phys. Plasmas* **4** (1997), 1654.
[40] D. De Lazzari and E. Westerhof, *Nucl. Fusion* **50** (2010) 079801.
[41] C. C. Hegna and J. D. Callen, *Phys. Plasmas* **4** (1997), 2940.
[42] J. Yang, *et al.*, *Phys. Plasmas* **17** (2010), 052309.
[43] V. Igochine, *et al.*, *Nucl. Fusion* **57** (2017) 036015.
[44] P. Mantica, *et al*., *Plasma Phys. Control. Fusion* **48** (2006) 385.
[45] Q. Yu and S. Günter, *Nucl. Fusion* **48** (2008) 065004.
[46] Q. Yu, *et al.*, *Phys. Plasmas* **11** (2004) 1960.
[47] F. A. Volpe, *et.al*, *Phy. Rev .Lett.* **115** (2015), 175002.